

# Thickness and Substrate Dependent Thin Film Growth of Picene and Impact on the Electronic Structure

Takuya Hosokai,<sup>\*,†</sup> Alexander Hinderhofer,<sup>‡,§</sup> Fabio Bussolotti,<sup>‡,||</sup> Keiichirou Yonezawa,<sup>‡</sup> Christopher Lorch,<sup>§</sup> Alexei Vorobiev,<sup>⊥</sup> Yuri Hasegawa,<sup>#</sup> Yoichi Yamada,<sup>#</sup> Yoshihiro Kubozoro,<sup>&</sup> Alexander Gerlach,<sup>§</sup> Satoshi Kera,<sup>‡,||</sup> Frank Schreiber,<sup>§</sup> and Nobuo Ueno<sup>‡</sup>

<sup>†</sup>National Institute of Advanced Industrial Science and Technology (AIST), Tsukuba Central 2, 1-1-1 Umezono, Tsukuba, Ibaraki 305-8568, Japan

<sup>‡</sup>The Division of Nanoscience, Graduate School of Advanced Integration Science, Chiba University, 1-33 Yayoi-cho, Inage-ku, Chiba 263-8522, Japan

<sup>§</sup>Institut für Angewandte Physik, Universität Tübingen, 72076 Tübingen, Germany

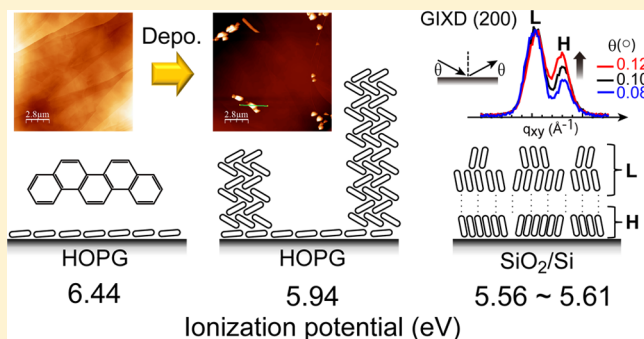
<sup>||</sup>Department of Photo-Molecular Science, Institute for Molecular Science, Myodaiji, Okazaki, Aichi 444-8585, Japan

<sup>⊥</sup>ESRF, 6 Rue Jules Horowitz, Boite Postale 220, 38043 Grenoble, Cedex 9, France

<sup>#</sup>Institute of Applied Physics, University of Tsukuba, 1-1-1 Tennodai, Tsukuba, Ibaraki 305-8573, Japan

<sup>&</sup>Research Laboratory for Surface Science, Okayama University, Okayama 700-8530, Japan

**ABSTRACT:** Thickness and substrate dependence of film growth, morphology, unit-cell structure, and electronic structures was thoroughly investigated for picene, the zigzag connected 5-ring molecule, by employing complementary techniques of *in situ* real-time X-ray reflectivity/diffraction, *in situ* electron spectroscopies, and atomic force microscopy. A different kind of thickness dependent structural transition was observed on SiO<sub>2</sub> and graphite, resulting in a distinct electronic structure. On SiO<sub>2</sub> picene films with 3D crystalline domains are formed with nearly upright molecular orientation from the initial growth stage. With increasing the film thickness the in-plane dimensions of the unit cell in the initially grown domains become smaller (in other words, more compressed), and, at the same time, crystalline domains with a more relaxed structure are nucleating on top of the compressed domains. In spite of such structural changes, the electronic structure, namely energy position of the highest occupied molecular orbital and threshold ionization potential (IP<sup>T</sup>), is not significantly altered. On graphite, on the other hand, we found a transition from a 2D (layer) to a 3D (island) growth mode with a variation of the molecular orientation from flat-lying to tilted one. The IP<sup>T</sup> changes significantly between the 2D and 3D growth regime in contrast to the SiO<sub>2</sub> system. The origin of the different IP<sup>T</sup>s of these picene thin films is discussed. The present results are compared with other planar  $\pi$ -conjugated compounds, in particular pentacene which is a structural isomer of picene and shows electronic properties strongly different from picene thin films.



## INTRODUCTION

For the past few decades organic semiconductors (OSCs) have attracted considerable attention owing to their applications in different device categories, such as organic light-emitting diodes, organic photovoltaic cells, and organic thin-film transistors (OTFTs).<sup>1–4</sup> Nowadays, it is generally known that the precise control of film structure, namely, molecular packing/crystal structure and film morphology, as well as the electronic structure of OSCs is a prerequisite for obtaining excellent charge transport properties in those devices.<sup>4–15</sup> For example, a hole mobility of 1–50 cm<sup>2</sup>/(V s) in single crystals of pentacene and rubrene is drastically decreased to  $\sim 10^{-5}$ – $10^{-6}$  cm<sup>2</sup>/(V s) in amorphous thin films applied in OTFTs.<sup>16–19</sup>

So far, significant efforts have been put into controlling the film growth and structure by modification of the substrate surface and tuning of growth conditions, such as growth temperature and deposition rate.<sup>5–7,20,21</sup> Compared to inorganics, the difficulty of controlling the film growth and structure of OSCs stems intrinsically from the structural anisotropy of the OSC molecules, large orientational degrees of freedom, and also from the subtle interplay between intermolecular interaction and substrate–molecule interaction. All of these concepts impact the film growth, crystallization,

Received: October 25, 2015

Revised: December 3, 2015

Published: December 3, 2015

and the resulting electronic structure of organic thin films.<sup>6</sup> Thus, fundamental studies were extensively conducted to understand the film-growth-related properties by employing X-ray scattering techniques, microscopy methods and electron spectroscopies.<sup>6,7,19–27</sup> However, the guideline to control those film properties from the viewpoint of the chemical structure of OSCs is not established in sufficient detail because of the lack of understanding the impact of different molecular symmetry on the film properties.

Here, we study the film growth, morphology, unit-cell structure, and their correlation to electronic structure of picene ( $C_{22}H_{14}$ , Figure 1a) thin films grown on  $SiO_2$  and highly

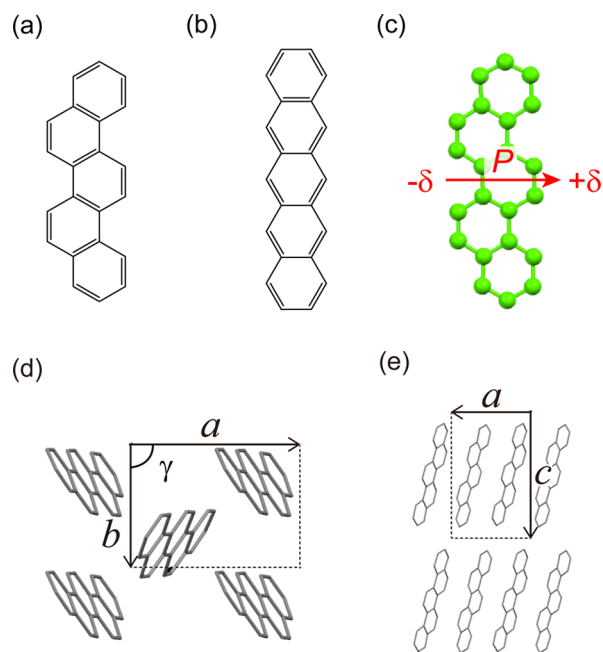


**Figure 1.** Chemical structure of picene (a) and pentacene (b). (c) Permanent molecular dipole moment ( $P$ ) (0.035 D) of picene calculated by density functional theory [B3LYP/6-311G\*\*] using the Gaussian 03W software package. Projection of unit cell structure from  $c$ -axis (d) and  $b$ -axis (e) and definition of an angle  $\gamma$ .  $P$  is canceled out in the single crystal unit cell.<sup>46</sup>

oriented pyrolytic graphite (HOPG) surfaces by X-ray reflectivity (XRR), grazing incidence X-ray diffraction (GIXD), two-dimensional GIXD (2D-GIXD), ultraviolet photoelectron spectroscopy (UPS), metastable atom electron spectroscopy (MAES), and atomic force microscopy (AFM). Picene is an isomer of the prototypical OSC pentacene (Figure 1b) and has a zigzag shape (symmetry:  $C_{2v}$ ) in contrast to the linear shape of pentacene (symmetry:  $D_{2h}$ ). Their distinct shapes lead to largely different physical and device properties: (1) Picene has a molecular dipole moment (0.035 D) along the short molecular axes (Figure 1c). (2) The optical band gap of picene is 3.31 eV, which is extremely high compared to pentacene (1.85 eV), originating in the different size of the  $\pi$ -conjugation systems.<sup>28,29</sup> (3) Picene single crystals doped with alkali metals show superconductivity at 18 K.<sup>30</sup> (4) A functionalization of the chemical structure is also possible, like alkyl-substituted picene, which has recently shown the highest hole carrier mobility in OTFTs of  $\sim 21 \text{ cm}^2/(\text{V s})$ .<sup>31</sup> (5) Picene-based OTFTs possess an oxygen gas sensing property.<sup>29,32</sup> (6) The experimentally determined width of the energy band dispersion of the single crystals are  $\sim 0.4 \text{ eV}$

(pentacene) and  $\sim 0.2 \text{ eV}$  (picene).<sup>11,14,33</sup> Regarding film structures, it is observed that both picene and pentacene form crystalline domains with upright standing orientations ( $S$ -orientation) on weakly interacting substrate surfaces, such as  $SiO_2$ .<sup>34,35</sup> However, compared to pentacene thin films, the growth and structure and the resulting electronic structure of picene thin films were not extensively studied. Both  $SiO_2$  and graphite surfaces are regarded as model inert surfaces to give a distinct film growth and molecular orientation for larger planar  $\pi$ -conjugated molecules. *In situ* and real-time XRR and (2D-)GIXD measurements can provide detailed information on film growth and crystal structures. Particularly, we address the structural transition of crystalline domains of picene during thin film growth. UPS and MAES are used to determine the valence band electronic structure of picene thin films. Different from UPS, MAES uses metastable He atoms as probes, which do not penetrate into the bulk of a solid, to enable the observation of the outermost surface electrons selectively and gives direct information on the orientation of the top molecular layer.<sup>36,37</sup> Therefore, the combination of UPS and MAES is also able to provide information on film growth and morphology, which is in particular useful for the HOPG systems.

## EXPERIMENT

Picene (purity: 99.9%) purchased from NARD Co Ltd. was used without further purification. For the substrates,  $Si(100)$  wafers covered with native oxide [root-mean-square (rms) surface roughness is 0.3 nm, and thickness of  $SiO_2$  is 1 nm, obtained by fitting XRR data with the MOTOFIT<sup>38</sup> by applying the Parratt formalism] and/or ZYA-grade HOPG were utilized. Before film growth the  $SiO_2$  substrates were cleaned ultrasonically with acetone, isopropyl alcohol, and ultrapure water, followed by heating to 700 K in the ultrahigh-vacuum (UHV) growth chamber (base pressure:  $\sim 10^{-8} \text{ Pa}$ ), while the HOPG substrates were cleaved *ex situ* and heated at 673 K for 24 h in the UHV chamber. The cleanness of the substrate surface was confirmed by measuring either XRR or UPS. On these substrates, we grew picene thin films and conducted the following *in situ* measurements, except AFM measurements, for which *ex situ* samples were used.

All the X-ray scattering experiments were performed at beamline ID10B<sup>39</sup> at the ESRF in Grenoble (France), using a home-built portable UHV chamber<sup>40</sup> at a wavelength of 0.925 Å. On the clean  $SiO_2$  surface, thin films of picene were prepared by organic molecular beam deposition at a substrate temperature of 303 K.<sup>5,6</sup> During the growth, we conducted real-time measurements of XRR and 2D-GIXD with an accumulation time of 1.5 min for XRR and 1 min for 2D-GIXD. For XRR and postgrowth GIXD we used a scintillation counter (Cyberstar), while a MarCCD area detector was used for 2D-GIXD. The deposition rate was set to 0.2–0.3 nm/min monitored by a water-cooled quartz crystal microbalance calibrated by XRR. For 2D-GIXD the angle ( $\theta$ ) of incidence relative to the sample surface was  $0.10^\circ$ . Lower limits of the in-plane coherent crystal sizes  $l_s$  were determined by the Scherrer formula  $l_s = 2\pi \times (\text{fwhm})^{-1} \times 0.9394 \times K_s$ , where  $K_s = 1.0747$  is the Scherrer constant for spherical grains and fwhm is the full-width half-maximum of the peak (in  $\text{\AA}^{-1}$ ) determined with a Gaussian fit-function.<sup>41</sup> The instrumental broadening of the diffractometer was not included in the calculation; therefore, only lower limits of  $l_s$  are given.

He I UPS and MAES were carried out using a home-built UHV system equipped with a PHOIBOS-HSA100 analyzer

(energy resolution was set to be 60 meV and a photoelectron acceptance angle of  $\pm 9^\circ$ ).<sup>37</sup> After cleaning the SiO<sub>2</sub> and HOPG surfaces, picene was deposited independently on those substrates kept at 295 K (deposition rate: 0.1–0.2 nm/min measured with a water-cooled quartz microbalance close to the substrates). After each deposition He I UPS and He\* (2<sup>3</sup>S) MAES experiments were carried out *in situ* in the analysis chamber under a measurement geometry with a light incident angle of 45° and an electron emission angle of 0° (normal emission) for UPS and of 30° for MAES. A detailed description of the MAES technique can be found in ref 36. During the UPS data collection a sample bias of –5 V was applied to the substrate to obtain the secondary cutoff (SECO) energy.

He I $\alpha$  UPS measurements were performed independently using an ultrahigh-sensitivity UPS apparatus with a hemispherical electron energy analyzer (MBS A-1) and a monochromatic He light source. The details of the apparatus are described in refs 42 and 43. All the He I $\alpha$  UPS spectra were measured at normal emission with an acceptance angle of  $\pm 18^\circ$  and a bias of –5 V. The energy resolution of the UPS system was set to 30 meV.

AFM measurements of the picene/HOPG systems were conducted in tapping mode under atmospheric pressure at room temperature, using S-image system (SII NanoTechnology). The AFM tips used here were SI-DF20 (Hitachi High-Tech Sci. Corp.), and the resonance frequency was 133 kHz.

## RESULTS AND DISCUSSION

**Picene on SiO<sub>2</sub>/Si Wafer.** The real-time XRR results of picene/SiO<sub>2</sub> system are shown in Figure 2a. Increasing the deposition time, in other words, increasing the film thickness ( $d$ ), results in a monotonic evolution of the (001) Bragg peak at  $q_z = 0.465 \text{ \AA}^{-1}$  ( $q_{\text{Bragg}}$ ), which corresponds to a lattice constant of 13.5 Å, demonstrating the formation of crystalline domains with S-orientation. Figure 2b shows the intensity variation at half of  $q_z$  of the Bragg peak ( $(1/2)q_{\text{Bragg}}$ ), which is the so-called anti-Bragg point, and also rms surface roughness estimated by fitting of XRR data in Figure 2a. According to the established real-time scattering formalism, the layer-by-layer growth shows intensity oscillations at  $(1/2)q_{\text{Bragg}}$ , and the roughening of the thin films reduces the amplitude of the oscillations.<sup>44</sup> In Figure 2b, the reflectivity at  $(1/2)q_{\text{Bragg}}$  decreases until  $\sim 5$  nm without any oscillation and then stays almost unchanged. This result reflects a strong roughening of picene thin films with no wetting layer formation, as predicted before by *ex situ* AFM measurements.<sup>45</sup> The strong roughening is also seen quantitatively in Figure 2b. The roughening, determined from the Kiessig oscillations, starts at around 3 nm similar as concluded from the anti-Bragg-point intensity.

Next, we focus on a transition of the in-plane unit cell structure observed via (2D-)GIXD. Figure 3a shows the real-time intensity evolution of GIXD patterns at the specular condition ( $q_z = 0.02 \text{ \AA}^{-1}$ ) obtained from real-time 2D-GIXD images. Also, the final image of the 2D-GIXD is shown in Figure 3b (right) with the postgrowth XRR result (left). Indexing of the diffraction peaks in Figures 3a and 3b was done according to a previous report referring to the unit cell of single crystals (see Figures 1d and 1e).<sup>46</sup> In Figure 3a four Bragg peaks, i.e., (110), (200), (210), and (020), are observed and become more intense until a critical  $d$  of  $\sim 8$  nm. Above  $\sim 8$  nm it is seen that the (200) and (210) reflections shift gradually to higher  $q_{xy}$  values, and at the same time new diffraction peaks appear at lower  $q_{xy}$  values. These results demonstrate the

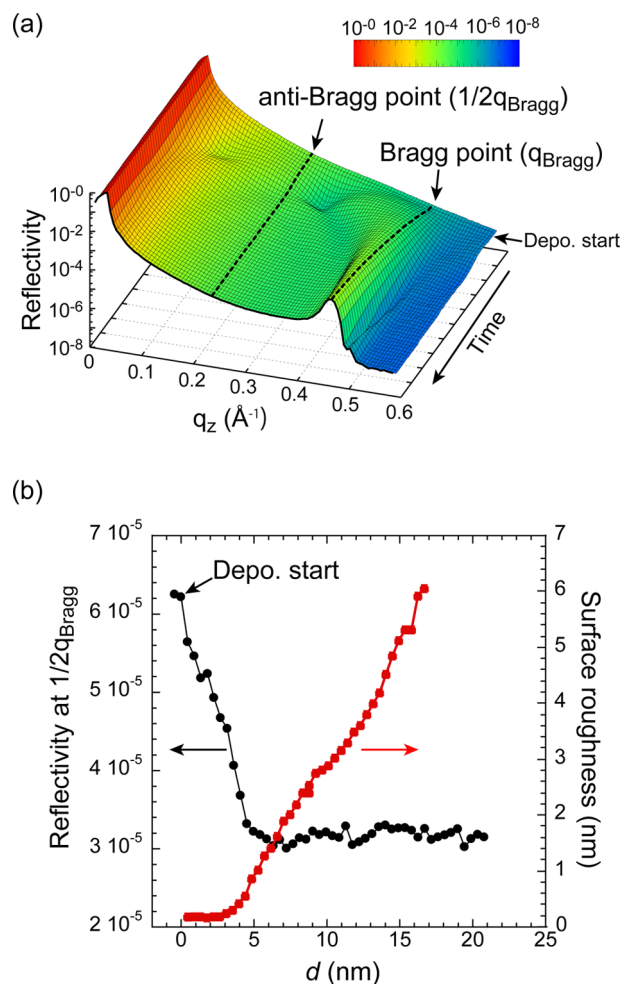


**Figure 2.** (a) Real-time XRR of picene thin film grown on SiO<sub>2</sub> showing the (001) Bragg reflection. (b) Intensity evolution at  $(1/2)q_{\text{Bragg}}$  and rms surface roughness at each  $d$  extracted from (a). For the roughness estimation reliable fitting results were obtained only up to  $d \approx 16$  nm due to the high roughness above this thickness.

thickness dependent structural transition of picene thin films during growth. The initially grown crystalline domains change their in-plane unit cell structure and at the same time crystalline domains having a different in-plane unit cell structure grow. Here, we denote the initially grown crystalline domains with I, and the later grown ones showing the (200) and (210) peaks at higher (or lower)  $q_{xy}$  as H (or L). A postgrowth 2D-GIXD image in Figure 3b exhibits crystal truncation rods along the  $q_z$  direction only for domains L, indicating the coherent ordering of the domains L along the  $q_z$  direction.

The appearance of the domain L above  $\sim 8$  nm shows that the growth of the domain L on top of the domain H that originates from the structural transition of domain I. To verify this, the  $\theta$  (incident angle) dependent specular GIXD measurements in the (200) and (210)  $q$ -region were conducted. Variation of  $\theta$  tunes the detection depth of GIXD either more to the surface (at lower  $\theta$ ) or more to the bulk regime (at higher  $\theta$ ) because the penetration depth of the evanescent X-ray field changes with  $\theta$  [penetration depth  $\sim \lambda / \{2\pi(\theta_c^2 - \theta^2)^{1/2}\}$ , where  $\lambda$  is the X-ray wavelength and  $\theta_c$  is the critical angle for the total reflection].<sup>47,48</sup> The results are shown in Figure 4, where the intensity is normalized to that of the domain L. It is clear that the diffracted intensity derived from

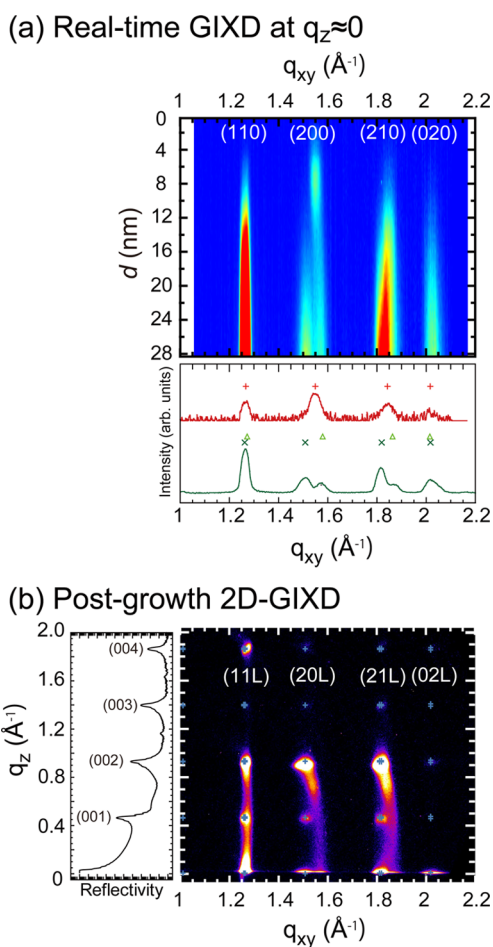


**Figure 3.** (a) Intensity evolution of GIXD of picene/SiO<sub>2</sub> systems taken from an image sequence of real-time 2D-GIXD. At the bottom, GIXD diffraction patterns at  $d = 8$  nm (red) and  $d = 28$  nm (green), which corresponds to thicknesses before and after the structural transition (see main text). Peak positions of the different domains are marked with + for domains of I, × for domains of L, and △ for domains of H. (b) The postgrowth XRR (left) and 2D-GIXD pattern (right).

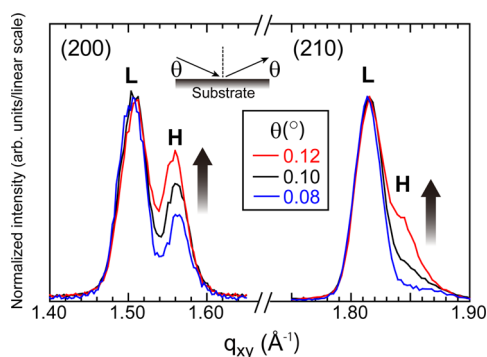


**Figure 4.**  $\theta$ -dependent intensity of (200) and (210) diffraction peaks. L and H peaks correspond to domains L and H, respectively.

the domain H increase with increasing the  $\theta$ . This result clearly indicates that the domains L are located at the surface region in the picene thin films, as considered above. A coherent island size  $l_s$ , which was estimated using the Scherrer formula, is 15.7 nm for domain L (top domain) and 17.6 nm for domain H (bottom domain).

The thickness dependent structural transition in the picene thin films is mainly probed by the (200) and (210) reflections, suggesting a prominent change of  $a$ -axis in the in-plane unit cell. To discuss the change quantitatively, we simulated the four diffraction positions of domain I, H, and L depicted in Figure 3a based on a monoclinic structure with a least-squares fitting routine (see ref 35). The results are summarized in Table 1,

**Table 1.** In-Plane Unit Cell Parameters of Domain I, H, and L and Also Single Crystals<sup>46</sup>

	$a$ (Å)	$b$ (Å)	$\gamma$ (deg)	in-plane area (Å <sup>2</sup> )
domain I	8.11	6.23	89.56	50.52
domain H	7.96	6.24	89.36	49.64
domain L	8.33	6.23	90.28	51.89
single crystal	8.480	6.154	90.46	52.18

where the corresponding unit-cell parameters of the picene single crystal structure are also listed.<sup>46</sup> From Table 1 it is clear that the  $a$ -axis varies strongly by 8.11, 7.96, and 8.33 Å for domains I, H, and L, while the  $b$ -axis is almost identical, 6.23–6.24 Å.  $\gamma$  is close to 90° within a deviation of 1° for all the domains and also the single crystal. The structural transition of domain I to domain H induces the shrinking of the  $a$ -axis, while the relaxed domain L grows on the stressed domain H. These results are summarized schematically in Figure 5.

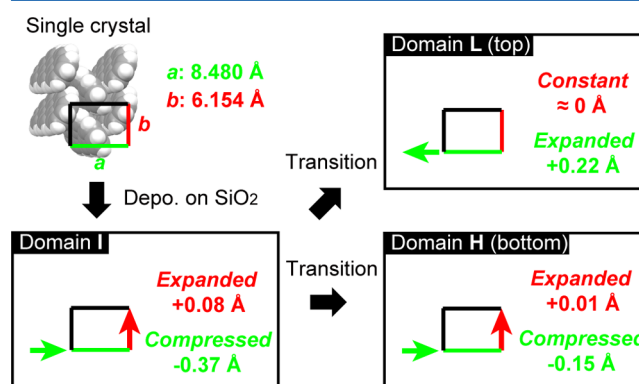


**Figure 5.** Schematics of the structural transition and in-plane unit cell structure of picene domains on SiO<sub>2</sub>.

Thickness dependent structural transitions have been reported for several OSCs on SiO<sub>2</sub> (or even on organic monolayers) and were discussed as one of the critical factors for film growth of OSCs.<sup>40,48–53</sup> As the reason for the transition, Hayakawa et al. have argued that the transition is induced by internal strain in the crystalline layer domains due to the presence of the substrate, and this strain is released with increasing  $d$ .<sup>52</sup> Furthermore, it was indicated that the presence of the strain causes the transition of growth mode from layer-by-layer to islands, i.e., Stranski–Krastanov growth mode.<sup>54</sup> However, our experimental results suggest that the existence of the strain in organic thin films is not always related to the 2D–3D growth transition, as picene grows with 3D islands with strain from the initial growth stage. As far as we know, picene is the first OSCs that show the structural transition upon the 3D-island growth mode.

Below, we discuss the impact of the structural transitions on the electronic structure of picene/SiO<sub>2</sub> systems. Figures 6a and 6b show the  $d$  dependence of UPS and MAES spectra. The

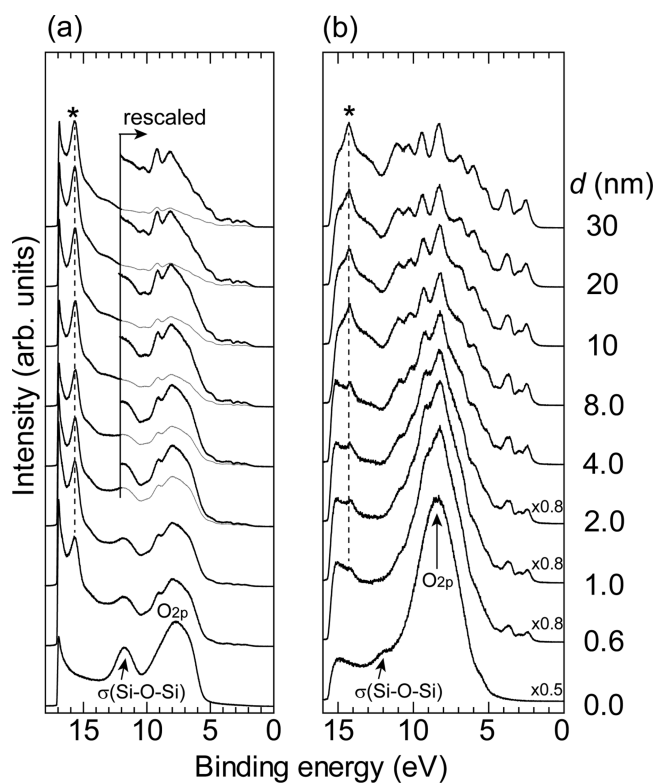


**Figure 6.** He I UPS (a) and MAES (b) spectra of picene/SiO<sub>2</sub> systems as a function of  $d$ .

lateral axes are binding energy ( $E_B$ ) with respect to the Fermi energy of an Au substrate, which was determined before and after the measurements for the energy calibration. A sharp feature (\*) in Figures 6a and 6b may be attributed to the high density-of-states of conduction bands of the picene thin films, as the same analogue to that reported for acene thin films with up-right standing orientation and high crystallinity.<sup>23</sup> Very broad features in the substrate spectra of UPS and MAES are ascribed to the nonbonding states of the O 2p orbitals of SiO<sub>2</sub> surface (O 2p) and the  $\sigma(\text{Si-O-Si})$  bonding state.<sup>55</sup> With increasing  $d$ , the intensity of the substrate features decreases gradually but still remains visible even at 8.0 nm, which is much larger than the detection depth of UPS and MAES. UPS can detect inelastic photoelectrons coming from the outmost surface to a depth of  $\sim 1$  nm, while MAES detects only electrons from the outermost surface.<sup>37</sup> This finding is in line with the growth scenario deduced from X-ray scattering experiments, i.e., picene grows in 3D domains without a wetting monolayer formation; otherwise, the formation of the monolayer (1.35 nm) should suppress the substrate features completely at  $d > 1.35$  nm.

Figures 7a and 7b show the expanded SECO and top band region of UPS in Figure 6a. Because of the 3D-island growth mode, photoelectrons from the substrate are contained in the thin film spectra (see Figure 6a); therefore, we subtracted the substrate contribution from the thin film spectra, and the results are redrawn in Figure 7c, together with UPS spectrum of a picene single crystal measured with the same configuration as shown in ref 33. For the subtractions the substrate spectrum was multiplied to fit the tail-like intensity seen below an energy of the threshold of the top band for each picene spectra in Figure 7b (see the example of the 0.6 nm spectrum). In contrast to the clear observation of the structural transitions, we

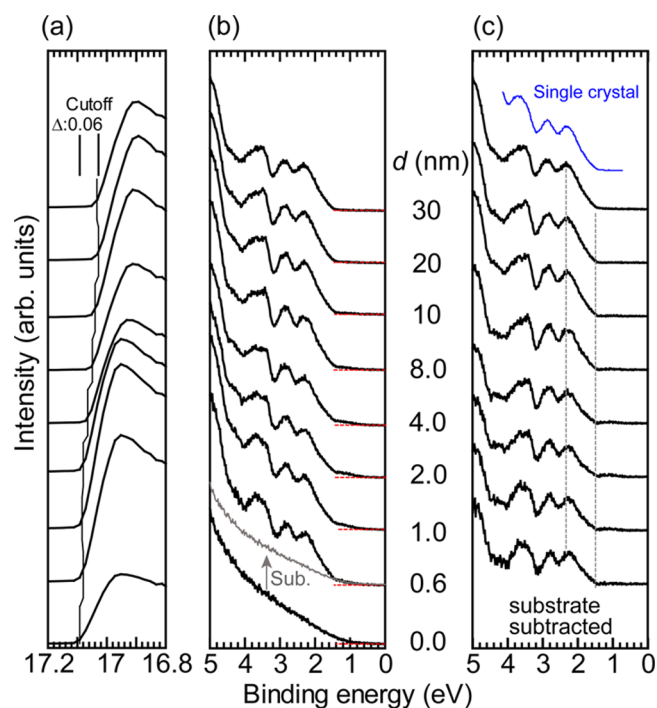


**Figure 7.**  $d$  dependent SECO (a) and top band region (b) in He I UPS spectra extracted from Figure 6a. (c) Redrawn of top band spectra after subtraction by the substrate spectrum. The top spectrum is that of the single crystal of picene taken from ref 33.

found only tiny changes in the UPS spectra dependent on  $d$ . In Figure 7a, the SECO position initially at  $E_B = 17.09$  eV decreases gradually, and the total shift ( $\Delta$ ) is  $-0.06$  eV at 20 nm. All thin film spectra in Figure 7c resemble the single crystal (see the top spectrum). The onset energy position of the top band of the thin films is 1.42 eV independent of  $d$ . Accordingly, the threshold ionization potential ( $\text{IP}^T$ ) of picene films, which is calculated from the SECO and onset position of the top band, is 5.56–5.61 eV in the present  $d$  range. The  $\text{IP}^T$  of 5.5 eV is also reported previously.<sup>29</sup> These results indicate that the electronic structure of picene thin films is not altered significantly by the structural transition.

Previously, Gottardi et al. have studied film morphology and growth of picene thin films fabricated by supersonic molecular beam deposition method. They observed screw-type dislocations on the surface of picene domains and the dislocations increased with increasing the film thickness.<sup>56</sup> Consequently, the density of terraces and the number of defects sites were also increased. Regarding such and further defects of OSC thin films, on the other hand, it was discussed by UPS studies that the structural defects induce gap states, which were observed as exponential tailing of the molecular top band reaching to the Fermi level in addition to Gaussian tailing near the top (HOMO) edge.<sup>57,58</sup> To discuss this point also for picene thin films, i.e., the structural defects induced gap states, we investigated the gap state region of picene thin films ( $d = 20$  nm) on SiO<sub>2</sub> by means of ultralow background, monochromatized UPS.<sup>42,43</sup> The results are shown in Figure 8, where the photoemission intensity at the vertical axis is converted to density-of-states (DOS) according to the refs 57 and 59. The high sensitivity of the present measurement is demonstrated for the SiO<sub>2</sub> spectrum, where the gap states near the Fermi level are clearly observed. In comparison, the thin film spectrum of picene shows only a much smaller density of gap states. At a

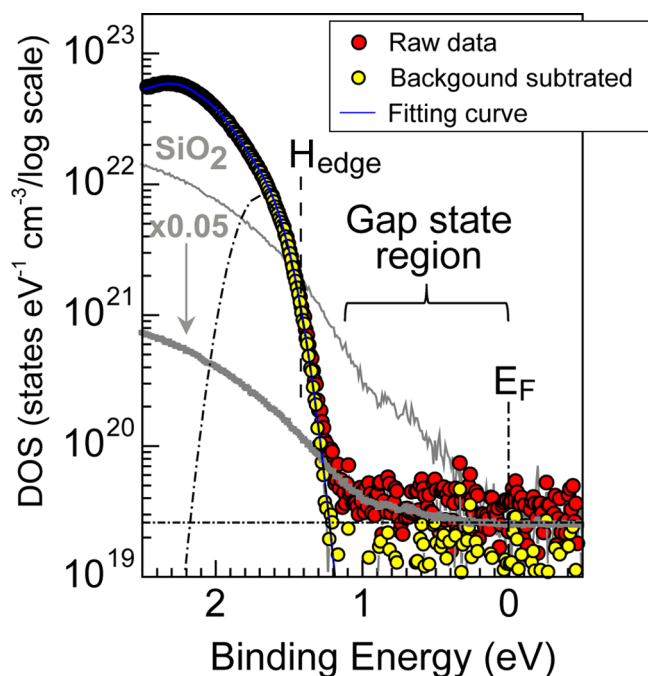


**Figure 8.** He I  $\alpha$  UPS spectra in gap state region of picene thin films ( $d = 20$  nm) on SiO<sub>2</sub> and the bare SiO<sub>2</sub>/Si substrate measured by the ultralow background, monochromatized UPS apparatus.<sup>42,43</sup> Fitting curve of the top band after the subtraction of substrate background is obtained by using series of Gaussians. DOS in the vertical axes is calculated according to refs 57 and 59. DOS at HOMO band edge in an intensity linear scale ( $H_{\text{edge}}$ ) is  $1.1 \times 10^{21}$  states  $\text{eV}^{-1} \text{cm}^{-3}$ .

film thickness  $d$  of 20 nm mostly domain L is expectedly present at the surface. We may therefore conclude that dislocations associated with domain L do not cause an increase in the gap state density.

In line with the previous reports based on *ex situ* AFM, we found a 3D-island growth mode from initial stages in the present experiments.<sup>45,56</sup> In this study we newly observed a complex structural transition from the initial film growth of picene; the domain I changes to domain H, and domain L starts to grow, presumably on top of domain H. While all kinds of the domains consist of molecules with *S*-orientation, the in-plane unit cell length of the domain H is reduced along the *a*-axis, while for the domain L it is increased with respect to the domain I. It was expected that the structural transition may influence the electronic structure of picene thin films. However, as investigated by UPS, no clear change in the SECO, the onset of the top band, and the IP<sup>T</sup> were observed. In this regard, the picene thin films seem to have rather different growth properties compared to pentacene thin films. Pentacene also forms thin films on SiO<sub>2</sub> with *S*-orientation from initial growth stages. However, pentacene can wet the SiO<sub>2</sub> surface completely and exhibits a change in growth mode from 2D to 3D.<sup>34,60,61</sup> X-ray scattering experiments have revealed that for the first monolayer and multilayers the in-plane unit cell structure varies, and even in the multilayer regime pentacene shows a structural transition known as polymorphous of thin film phase and bulk phase.<sup>34,51,62</sup> Thickness dependent UPS measurements reflect such complex structural changes. Fukagawa et al. showed that the first monolayer of pentacene has broad top band features.<sup>23</sup> For thicker films the top band shape is split due to the formation of energy band dispersion in the crystalline domains, which could be attributed to the thin

film phase.<sup>23,63</sup> Yoshida et al. investigated the valence top band of the bulk phase by preparing a very thick ( $d = 250$  nm) pentacene film and obtained spectral shape distinct from the thin film phase due to a large difference in their unit cell structures.<sup>11</sup> Both the spectral shape of the thin film phase and bulk phase including energy band dispersion could be realized even in one monolayer if appropriate substrate surfaces are chosen.<sup>23,64,65</sup> In this regard, it is understood that the electronic structure does not depend on  $d$  and is determined by the crystallinity, packing structure, and molecular orientation, except energy level alignment issues (formation of interfacial dipole), which could be avoided by using an inert surface, like in the case of SiO<sub>2</sub> and HOPG. Actually, the isotropic compound fullerene (C60) exhibits nearly identical UPS spectra for uniaxially ordered and nonordered thin films except for the interface to the underlying substrates.<sup>27,66</sup> Taking this consideration into account for the present UPS results in Figures 7, it is concluded that the structural transitions among the domains I, H, and L do not have a large impact on the electronic structure of picene thin films because of their high crystallinity, identical *S*-orientation, and similar unit-cell structure. Unlike pentacene, we suppose that those domains are basically not polymorph and result from stress driven internal rotations of picene molecules in the unit cell.

**Picene on HOPG.** Figures 9a and 9b show the  $d$  dependence of UPS and MAES spectra of picene thin films

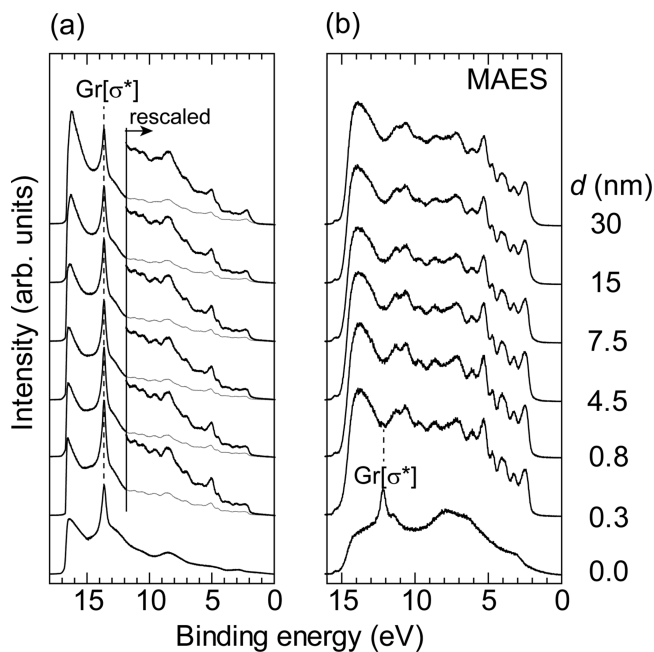


**Figure 9.** He I UPS and MAES spectra of picene/HOPG systems as a function of  $d$ : all region for UPS (a) and MAES (b). The sharp feature Gr[ $\sigma^*$ ] stems from the conduction bands of the graphite surface.

on HOPG. In MAES, the signal of the conduction band of the graphite at  $E_B = 12.2$  eV (Gr[ $\sigma^*$ ]) is barely observed at  $d = 0.3$  nm, while the corresponding band remains visible in UPS. This demonstrates that the substrate surface is almost fully covered by the picene molecules at 0.3 nm because He\* atoms do not penetrate into the bulk of the solid and instead selectively excite electrons at the outermost surface.<sup>37</sup> It also means that the film growth is rather different to the picene/SiO<sub>2</sub> system, which exhibited a strong 3D island growth, requiring very thick films

( $d \sim 20$  nm) to fully cover the substrate surface. For higher  $d$ s no remarkable changes are observed in either the UPS or MAES spectrum. Note that the  $\text{Gr}[\sigma^*]$  band in UPS remains very strong even at  $d = 30$  nm, suggesting that a very thin region still exists even at this  $d$ .

To confirm the film morphology, we conducted *ex situ* AFM of picene/HOPG systems. The AFM image of the monolayer film of picene ( $d \sim 0.3$  nm) in Figure 10a depicts a

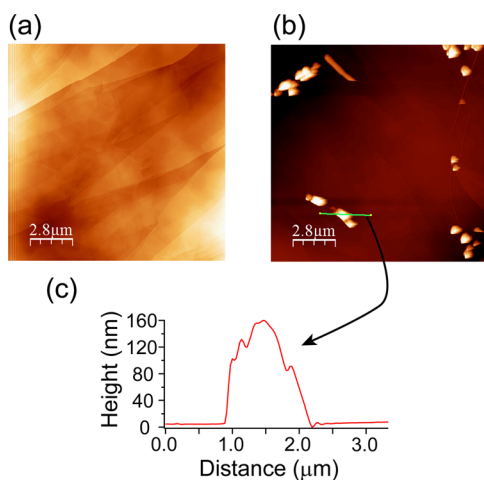


**Figure 10.** *Ex situ* AFM images ( $14.5 \times 14.5 \mu\text{m}$ ) of picene/HOPG systems: (a)  $d \sim 0.3$  nm; (b)  $d \sim 1$  nm. (c) A height profile along the line drawn in the image (b).

homogeneous morphology with clear steps of the graphite layers. For the multilayer coverages ( $d \sim 1$  nm) in Figure 10b, molecular domains with extremely large thickness are observed additionally, as it is obvious from the height profile of one of the domains in Figure 10c. These findings lead to a conclusion that picene forms dewetting 3D multilayer domains on the underlying first wetting monolayer.

To elaborate the impact of the film growth on the spectral evolution of the UPS spectra, we focus on the SECO and top band region observed by UPS in Figures 11a and 11b. In Figure 11a the SECO position of HOPG is observed at 16.80 eV and is shifted to 16.73 eV at the monolayer coverage ( $d = 0.3$  nm). Such a small shift of the SECO position has also been observed and suggested to originate in the permanent dipole moment of picene molecules inclined slightly relative to the substrate surface.<sup>67</sup> The SECO position of the monolayer coverage stays unchanged up to 7.5 nm. For the higher  $d$ s, the SECO position is shifted again to 16.65 eV at the final  $d$  of 30 nm. Following the SECO position, we also found a significant change in the top band features. In Figure 11b, the top band at the final  $d$  is apparently sharper than that of the monolayer spectrum. Furthermore, the spectrum at  $d = 30$  nm contains a larger tailing of the intensity to the lower  $E_B$  side. To judge the observed changes, we subtracted the substrate contribution as performed for the picene/ $\text{SiO}_2$  system in Figure 7c, and the results are shown in Figure 11c. It is clear that above 7.5 nm the top band region shows new features at the lower  $E_B$  side (see the top spectrum). Because of the appearance of the new features, the onset energy of the top band of the monolayer is shifted from 1.94 to 1.37 eV. As a result, we find a change of the  $\text{IP}^T$  from 6.44 eV for the monolayer regime to 5.94 eV for the thicker regime. This result indicates that the domain structure in the multilayer regime is different from that of the monolayer,

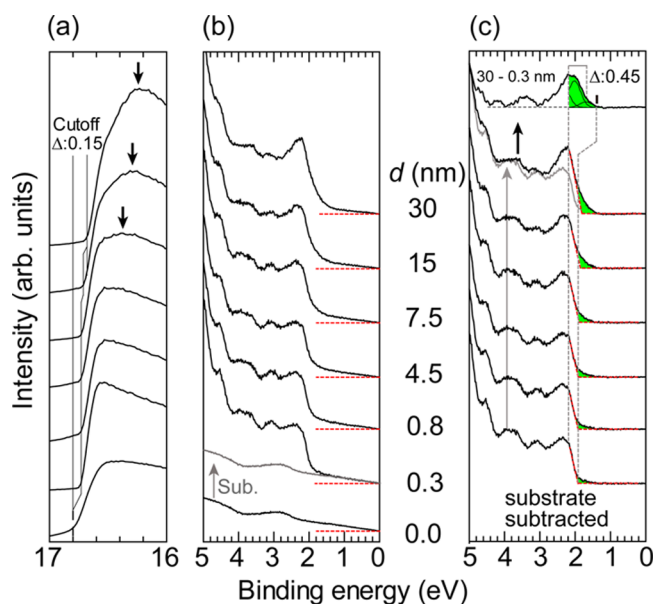


**Figure 11.** He I UPS spectra of picene/HOPG systems as a function of  $d$ : SECO (a) and top band region (b). (c) Top band spectra after subtraction of the substrate spectrum. The top band spectrum is the 30 nm spectrum subtracted by the 0.3 nm spectrum for better visualization of the differences. The residue in the top spectrum was fitted with Gauss functions.

since the  $\text{IP}^T$  is a fingerprint of the film structure of organic thin films as will be discussed below.

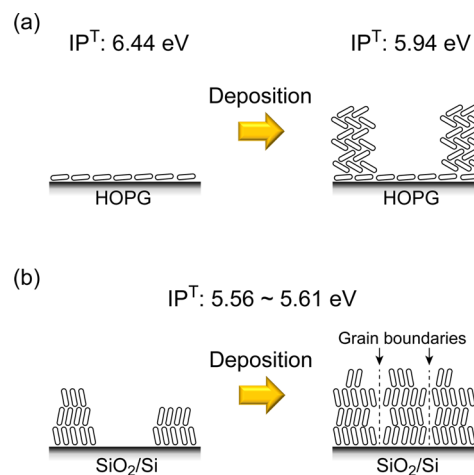


**Figure 12.** Schematic of the growth model of picene thin films on HOPG (a) and on  $\text{SiO}_2$  (b) surface: Left-hand side shows the initial growth stage, and the right-hand side is the final growth stage.

**A Comparison of Film Structure and Electronic Structure of Picene on HOPG and  $\text{SiO}_2$ .** Figures 12a and 12b summarize the  $\text{IP}^T$  and film structure of the picene/HOPG and  $\text{SiO}_2$  systems in the initial and final growth stages. Here, we discuss the origin of the observed  $\text{IP}^T$  differences of picene thin films in the present results. The factors which affect the  $\text{IP}^T$  of organic thin films are usually explained by surface dipole moment, permanent molecular dipole moment, energy band dispersion, and molecular packing/crystal structures (final-state photohole screening effect).<sup>23,68</sup> Any of them are affected by molecular orientation, and thus orientation-dependent  $\text{IP}^T$  is often observed. For example, pentacene films showed  $\text{IP}^T$  of

5.45 eV for a flat-lying orientation (*L*-orientation) on HOPG and 4.77 eV for *S*-orientation on SiO<sub>2</sub>.<sup>23</sup> The energy difference is 0.68 eV. These orientation-dependent IP<sup>T</sup>s have been ascribed to the electrostatic potential due to polar bonds of organic molecules, such as C<sup>δ-</sup>-H<sup>δ+</sup>.<sup>68</sup> The impact of the potential is reversed for perfluorinated organic molecules because of the inverse polarity of C<sup>δ+</sup>-F<sup>δ-</sup> bonds.<sup>69,70</sup> For picene, we found an IP<sup>T</sup> of 5.56 eV for *S*-orientation on SiO<sub>2</sub> and of 6.44 eV for (slightly inclined) *L*-orientation on HOPG. We thus obtained an energy difference of 0.89 eV and that the change is in line with the scenario of the orientation-dependent IP<sup>T</sup> since the *S*-orientation of picene, for which C<sup>δ-</sup>-H<sup>δ+</sup> bonds are located at the outermost surface, should decrease the IP<sup>T</sup> relative to one of *L*-orientation. We note that the value of the IP<sup>T</sup> difference is relatively high among OSCs reported so far.<sup>68</sup> As the reason, various factors can be considered as follows. A small permanent molecular dipole (0.035 D) of picene may contribute to the increase of the IP<sup>T</sup> of picene monolayers on HOPG because the SECO position is shifted in that direction from the bare surface (see Figure 11a). The energy band dispersion is expected to contribute the decrease of IP<sup>T</sup> for the *S*-orientation of picene on SiO<sub>2</sub> due to the similarity of the UPS spectrum as well as the unit cell structure to those of single crystals.<sup>33</sup> Final-state photohole screening, which is a molecular packing effect, could be also considered in picene and pentacene although the packing density of both compounds is similar (1.3–1.4 g/cm<sup>3</sup>).<sup>46,71</sup> Apart from the simplest consideration of the screening effects by the density only, more complex models were described as the extra-atomic relaxation energy depends for example on the (anisotropic) dielectric constant of the environment, which is not necessarily the same for both molecules. A recent paper by Yoshida et al. based on experimentally determined IP and electron affinity suggests that the polarization energy is largely orientation dependent and is a crucial factor for the orientation dependent IPs.<sup>72</sup> Since electron affinity of picene thin films is not clear yet, we do not go into the quantitative discussion for the larger IP<sup>T</sup> difference of picene based on the above two models, i.e., surface dipole vs polarization energy. But the large difference in IP<sup>T</sup>s of picene thin films would be worth to further study to deeply understand the phenomena of the orientation dependent IP<sup>T</sup> of OSCs.

The IP<sup>T</sup> of a multilayer film of pentacene on HOPG is 5.15 eV, which is in between those of the *S*- and *L*-orientations.<sup>23</sup> Götzen et al. investigated the structure of pentacene thin films in detail and reached to the conclusion that the *L*-oriented pentacene molecules in the first monolayer are lifted up when the second layer is formed.<sup>73</sup> The same phenomenon of lifting up in the monolayer regime is also suggested for picene and tetracene on Ag(111).<sup>74,75</sup> For such a crystal orientation, pentacene molecules tilt their shorter axes relative to the substrate surface by ca. 55°, and thus the IP<sup>T</sup> of the tilting phase would be in between that of the two orientations according to the above-mentioned orientational effect.<sup>69,73</sup> For the case of picene, the IP<sup>T</sup> of 5.94 eV of the multilayers on HOPG is also in between that of the *S*- and *L*-orientations. Analogous to pentacene, we could thus expect that picene grows with tilting orientation at higher *d*s on HOPG (Figure 12a), as the evidence of the decreasing IP<sup>T</sup> in the multilayer domains. Note that the IP<sup>T</sup> evaluated for the thicker regime would be the upper limit because the multilayer domains are not fully covering the first monolayer, and thus the SECO could shift further to decrease the IP<sup>T</sup>. The substrate dependent molecular

orientation of picene on SiO<sub>2</sub> and HOPG is basically the same as for pentacene.<sup>23</sup> Nevertheless, our studies imply that intermolecular interactions of picene in terms of film growth are rather different because picene tends to grow in 3D islands on both HOPG and SiO<sub>2</sub>. Since there are several possibilities of the crystal orientation, the detailed investigation of the multilayer structure is required as Götzen et al. concluded.<sup>73</sup>

Finally, we comment on the origin of distinct orientations of picene on HOPG and SiO<sub>2</sub>, namely, *L*- and *S*-orientation. In general, it is known that the polyaromatic hydrocarbons adsorb on HOPG with *L*-orientation and on SiO<sub>2</sub> with *S*-orientation. The situation is similar for hexa-peri-hexabenzocoronene (HBC) molecules, a discotic, polycyclic hydrocarbon that can be considered as a hydrogen-terminated molecular version of graphene, the so-called nano-graphene.<sup>76</sup> Beyer et al. deposited HBC on SiO<sub>2</sub>, HOPG, and defect-rich HOPG, which was prepared by ion sputtering and be also regarded as atomically rough graphite surface. HBC molecules showed the same behavior as other planar  $\pi$ -conjugated molecules, i.e., *L*-orientation on HOPG and *S*-orientation on SiO<sub>2</sub>. However, notably, HBC adsorbed with *S*-orientation on the defective HOPG. For this reason, Beyer et al. pointed out the importance of coherence size of the underlying graphite surface structure for the HBC. The same concept can be adopted for picene molecules, since picene could be also regarded as a piece of surface layer of graphite similar to graphene.<sup>77</sup> Nevertheless, we note that the coherent size may be one of the key factors to affect the molecular orientation; the change in molecular orientation in terms of the substrate surface roughness was also observed for other substrates, such as hydrogen-terminated Si wafer and gold, with different organic  $\pi$ -conjugate molecules.<sup>78–80</sup> In addition to the substrate–molecule interaction, intermolecular interaction should also play a role in general. Thus, to clarify the origin of the substrate dependent molecular orientation of picene, further investigations are needed. Particularly, the substrate–molecule/intermolecular interactions and the roughness effect have to be comprehensively understood, which may need other complementary techniques, such as scanning tunneling microscopy, thermal desorption spectroscopy and the computational simulation to discuss the interaction energies quantitatively.

## CONCLUSIONS

In conclusion, we have studied the film growth, morphology, crystal structure and electronic structure of picene thin films on SiO<sub>2</sub> and HOPG surfaces with complementary techniques (X-ray scattering/diffraction, electron spectroscopy, and *ex situ* AFM). We found a substrate and thickness dependent molecular orientation and film growth: a 3D–2D growth transition on SiO<sub>2</sub> and 2D–3D growth transition on HOPG. On SiO<sub>2</sub>, the in-plane unit cell structure of picene changes by increasing the film thickness while keeping the *S*-orientation. However, UPS measurements reveal that the structural changes do not alter the electronic structure significantly, which may be caused by the high crystallinity and the identical orientation of the molecules before/after the structural transitions. On HOPG, very high 3D-islands are grown on the first wetting layer of picene molecules. We found a change in electronic structure for the picene/HOPG systems dependent on *d*, as the IP<sup>T</sup> of the monolayer is higher than that of the multilayer domains. Including the IP<sup>T</sup> of the picene on SiO<sub>2</sub>, we have discussed the origin of the IP<sup>T</sup> difference of picene observed on SiO<sub>2</sub> and HOPG.

The comparison to pentacene, the isomer of picene, suggests that while the molecular orientation on both substrates is basically the same, film growth is apparently different in particular for SiO<sub>2</sub>, where pentacene forms a wetting layer starting from the first monolayer. From this evidence, it is implied that intermolecular interactions are rather different between picene and pentacene, which is attributed to their different chemical structure and more specifically to their molecular symmetry. The present paper should contribute to the further understanding of the correlations between film growth and electronic structure of OSCs. Especially, the detailed understanding of intermolecular interactions in terms of the zigzag versus straight chemical structure of picene and pentacene, which corresponds to the switching between dipole vs. quadrupole intermolecular interaction, may be a key to control the film growth more precisely.

## AUTHOR INFORMATION

### Corresponding Author

\*E-mail: t.hosokai@aist.go.jp (T.H.).

### Notes

The authors declare no competing financial interest.

## ACKNOWLEDGMENTS

We acknowledge Rintaro Makino (Chiba university) for his experimental support of UPS and MAES. This research has been supported by JSPS KAKENHI Grants 25870034, 24245034 and 26248062, and Global-COE program at Chiba University (G-03, MEXT).

## REFERENCES

- (1) Tang, C. W. Two-Layer Organic Photovoltaic Cell. *Appl. Phys. Lett.* **1986**, *48*, 183.
- (2) Tang, C. W.; Vanslyke, S. A. Organic Electroluminescent Diodes. *Appl. Phys. Lett.* **1987**, *51*, 913.
- (3) Koezuka, H.; Tsumura, A.; Ando, T. Field-Effect Transistor with Polythiophene Thin Film. *Synth. Met.* **1987**, *18*, 699–704.
- (4) Brütting, W.; Adachi, C. *Physics of Organic Semiconductors*, 2nd ed.; Wiley VCH-Verlag: Weinheim, 2012.
- (5) Witte, G.; Wöll, C. Growth of Aromatic Molecules on Solid Substrates for Applications in Organic Electronics. *J. Mater. Res.* **2004**, *19*, 1889–1916.
- (6) Schreiber, F. Organic Molecular Beam Deposition: Growth Studies beyond the First Monolayer. *Phys. Status Solidi* **2004**, *201*, 1037–1054.
- (7) Koch, N.; Vollmer, A.; Salzmann, I.; Nickel, B.; Weiss, H.; Rabe, J. P. Evidence for Temperature-Dependent Electron Band Dispersion in Pentacene. *Phys. Rev. Lett.* **2006**, *96*, 156803.
- (8) Coropceanu, V.; Cornil, J.; da Silva Filho, D. A.; Olivier, Y.; Silbey, R.; Brédas, J.-L. Charge Transport in Organic Semiconductors. *Chem. Rev.* **2007**, *107*, 926–952.
- (9) Shirota, Y.; Kageyama, H. Charge Carrier Transporting Molecular Materials and Their Applications in Devices. *Chem. Rev.* **2007**, *107*, 953–1010.
- (10) Ueno, N.; Kera, S. Electron Spectroscopy of Functional Organic Thin Films: Deep Insights into Valence Electronic Structure in Relation to Charge Transport Property. *Prog. Surf. Sci.* **2008**, *83*, 490–557.
- (11) Yoshida, H.; Sato, N. Crystallographic and Electronic Structures of Three Different Polymorphs of Pentacene. *Phys. Rev. B: Condens. Matter Mater. Phys.* **2008**, *77*, 235205.
- (12) Kera, S.; Ueno, N. First Principles Measurements of Charge Mobility in Organic Semiconductors: Valence Hole-Vibration Coupling in Organic Ultrathin Films. *Prog. Surf. Sci.* **2009**, *84*, 135–154.
- (13) Machida, S.; Nakayama, Y.; Duhm, S.; Xin, Q.; Funakoshi, A.; Ogawa, N.; Kera, S.; Ueno, N.; Ishii, H. Highest-Occupied-Molecular-Orbital Band Dispersion of Rubrene Single Crystals as Observed by Angle-Resolved Ultraviolet Photoelectron Spectroscopy. *Phys. Rev. Lett.* **2010**, *104*, 156401.
- (14) Nakayama, Y.; Uragami, Y.; Machida, S.; Koswattage, K. R.; Yoshimura, D.; Setoyama, H.; Okajima, T.; Mase, K.; Ishii, H. Full Picture of Valence Band Structure of Rubrene Single Crystals Probed by Angle-Resolved and Excitation-Energy-Dependent Photoelectron Spectroscopy. *Appl. Phys. Express* **2012**, *5*, 111601.
- (15) Yanagisawa, H.; Tamaki, T.; Nakamura, M.; Kudo, K. Structural and Electrical Characterization of Pentacene Films on SiO<sub>2</sub> Grown by Molecular Beam Deposition. *Thin Solid Films* **2004**, *464–465*, 398–402.
- (16) Lee, J. Y.; Roth, S.; Park, Y. W. Anisotropic Field Effect Mobility in Single Crystal Pentacene. *Appl. Phys. Lett.* **2006**, *88*, 252106.
- (17) Seo, S.; Park, B.-N.; Evans, P. G. Ambipolar Rubrene Thin Film Transistors. *Appl. Phys. Lett.* **2006**, *88*, 232114.
- (18) Takeya, J.; Yamagishi, M.; Tominari, Y.; Hirahara, R.; Nakazawa, Y.; Nishikawa, T.; Kawase, T.; Shimoda, T.; Ogawa, S. Very High-Mobility Organic Single-Crystal Transistors with In-Crystal Conduction Channels. *Appl. Phys. Lett.* **2007**, *90*, 102120.
- (19) Chang, H.; Li, W.; Tian, H.; Geng, Y.; Wang, H.; Yan, D.; Wang, T. High Performance of Rubrene Thin Film Transistor by Weak Epitaxy Growth Method. *Org. Electron.* **2015**, *20*, 43–48.
- (20) Käfer, D.; Witte, G. Growth of Crystalline Rubrene Films with Enhanced Stability. *Phys. Chem. Chem. Phys.* **2005**, *7*, 2850–2853.
- (21) Käfer, D.; Ruppel, L.; Witte, G.; Wöll, C. Role of Molecular Conformations in Rubrene Thin Film Growth. *Phys. Rev. Lett.* **2005**, *95*, 166602.
- (22) Kowarik, S.; Gerlach, A.; Sellner, S.; Schreiber, F.; Pflaum, J.; Cavalcanti, L.; Konovalov, O. Anomalous Roughness Evolution during Growth of Rubrene Thin Films. *Phys. Chem. Chem. Phys.* **2006**, *8*, 1834–1836.
- (23) Fukagawa, H.; Yamane, H.; Kataoka, T.; Kera, S.; Nakamura, M.; Kudo, K.; Ueno, N. Origin of the Highest Occupied Band Position in Pentacene Films from Ultraviolet Photoelectron Spectroscopy: Hole Stabilization versus Band Dispersion. *Phys. Rev. B: Condens. Matter Mater. Phys.* **2006**, *73*, 245310.
- (24) Kowarik, S.; Gerlach, A.; Schreiber, F. Organic Molecular Beam Deposition: Fundamentals, Growth Dynamics, and In-Situ Studies. *J. Phys.: Condens. Matter* **2008**, *20*, 184005.
- (25) Hosokai, T.; Machida, H.; Kera, S.; Gerlach, A.; Schreiber, F.; Ueno, N. Impact of Structural Imperfections on the Energy Level Alignment in Organic Films. *Phys. Rev. B: Condens. Matter Mater. Phys.* **2011**, *83*, 195310.
- (26) Matsubara, R.; Sakai, M.; Kudo, K.; Yoshimoto, N.; Hirosawa, I.; Nakamura, M. Crystal Order in Pentacene Thin Films Grown on SiO<sub>2</sub> and its Influence on Electronic Band Structure. *Org. Electron.* **2011**, *12*, 195–201.
- (27) Hinderhofer, A.; Gerlach, A.; Broch, K.; Hosokai, T.; Yonezawa, K.; Kato, K.; Kera, S.; Ueno, N.; Schreiber, F. Geometric and Electronic Structure of Templated C<sub>60</sub> on Diindenoperylene Thin Films. *J. Phys. Chem. C* **2013**, *117*, 1053–1058.
- (28) Hinderhofer, A.; Heinemeyer, U.; Gerlach, A.; Kowarik, S.; Jacobs, R. M. J.; Sakamoto, Y.; Suzuki, T.; Schreiber, F. Optical Properties of Pentacene and Perfluoropentacene Thin Films. *J. Chem. Phys.* **2007**, *127*, 194705.
- (29) Okamoto, H.; Kawasaki, N.; Kaji, Y.; Kubozono, Y.; Fujiwara, A.; Yamaji, M. Air-Assisted High-Performance Field-Effect Transistor with Thin Films of Picene. *J. Am. Chem. Soc.* **2008**, *130*, 10470–10471.
- (30) Mitsuhashi, R.; Suzuki, Y.; Yamanari, Y.; Mitamura, H.; Kambe, T.; Ikeda, N.; Okamoto, H.; Fujiwara, A.; Yamaji, M.; Kawasaki, N.; et al. Superconductivity in Alkali-Metal-Doped Picene. *Nature* **2010**, *464*, 76–79.
- (31) Okamoto, H.; Hamao, S.; Goto, H.; Sakai, Y.; Izumi, M.; Gohda, S.; Kubozono, Y.; Eguchi, R. Transistor Application of Alkyl-Substituted Picene. *Sci. Rep.* **2014**.

- (32) Sugawara, Y.; Ogawa, K.; Goto, H.; Oikawa, S.; Akaike, K.; Komura, N.; Eguchi, R.; Kaji, Y.; Gohda, S.; Kubozono, Y. O<sub>2</sub>-Exposure and Light-Irradiation Properties of Picene Thin Film Field-Effect Transistor: A New Way toward O<sub>2</sub> Gas Sensor. *Sens. Actuators, B* **2012**, *171–172*, 544–549.
- (33) Xin, Q.; Duhm, S.; Bussolotti, F.; Akaike, K.; Kubozono, Y.; Aoki, H.; Kosugi, T.; Kera, S.; Ueno, N. Accessing Surface Brillouin Zone and Band Structure of Picene Single Crystals. *Phys. Rev. Lett.* **2012**, *108*, 226401.
- (34) Ruiz, R.; Choudhary, D.; Nickel, B.; Toccoli, T.; Chang, K.-C.; Mayer, A. C.; Clancy, P.; Blakely, J. M.; Headrick, R. L.; Iannotta, S.; et al. Pentacene Thin Film Growth. *Chem. Mater.* **2004**, *16*, 4497–4508.
- (35) Hosokai, T.; Hinderhofer, A.; Vorobiev, A.; Lorch, C.; Watanabe, T.; Koganezawa, T.; Gerlach, A.; Yoshimoto, N.; Kubozono, Y.; Schreiber, F. In-Situ Structural Characterization of Picene Thin Films by X-Ray Scattering: Vacuum Versus O<sub>2</sub> Atmosphere. *Chem. Phys. Lett.* **2012**, *544*, 34–38.
- (36) Harada, Y.; Masuda, S.; Ozaki, H. Electron Spectroscopy Using Metastable Atoms as Probes for Solid Surfaces. *Chem. Rev.* **1997**, *97*, 1897–1952.
- (37) Hosokai, T.; Horie, M.; Aoki, T.; Nagamatsu, S.; Kera, S.; Okudaira, K. K.; Ueno, N. Change in Molecular Conformation of Dibenzo-Crown Ether Induced by Weak Molecule-Substrate Interaction. *J. Phys. Chem. C* **2008**, *112*, 4643–4648.
- (38) Nelson, A. Co-Refinement of Multiple-Contrast Neutron/X-ray Reflectivity Data Using MOTOFIT. *J. Appl. Crystallogr.* **2006**, *39*, 273–276.
- (39) Smilgies, D.-M.; Boudet, N.; Struth, B.; Kononov, O. Troika II: A Versatile Beamline for the Study of Liquid and Solid Interfaces. *J. Synchrotron Radiat.* **2005**, *12*, 329–339.
- (40) Hosokai, T.; Gerlach, A.; Hinderhofer, A.; Frank, C.; Ligorio, G.; Heinemeyer, U.; Vorobiev, A.; Schreiber, F. Simultaneous In Situ Measurements of X-Ray Reflectivity and Optical Spectroscopy during Organic Semiconductor Thin Film Growth. *Appl. Phys. Lett.* **2010**, *97*, 063301.
- (41) Birkholz, M. *Thin Film Analysis by X-Ray Scattering*; Wiley-VCH: Weinheim, Germany, 2006.
- (42) Ishii, H.; Kudo, K.; Nakayama, T.; Ueno, N. *Electronic Processes in Organic Electronics: Bridging Nanostructure, Electronic States and Device Properties*; Springer-Verlag: Berlin, Germany, 2015; pp 51–67.
- (43) Bussolotti, F. High-Sensitivity Ultraviolet Photoemission Spectroscopy Technique for Direct Detection of Gap States in Organic Thin Films. *J. Electron Spectrosc. Relat. Phenom.* **2015**, *204*, 29–38.
- (44) Kowarik, S.; Gerlach, A.; Skoda, M.; Sellner, S.; Schreiber, F. Measurement and Analysis of X-Ray Growth Oscillations beyond the Anti-Bragg Point. *Eur. Phys. J.: Spec. Top.* **2009**, *167*, 11–18.
- (45) Kurihara, R.; Hosokai, T.; Kubozono, Y. Growth and Structure of Picene Thin Films on SiO<sub>2</sub>. *Mol. Cryst. Liq. Cryst.* **2013**, *580*, 83–87.
- (46) Ghosh, R.; Roychowdhury, S.; Roychowdhury, P. Structural Analysis of Picene, C<sub>22</sub>H<sub>14</sub>. *Acta Crystallogr., Sect. C: Cryst. Struct. Commun.* **1985**, *41*, 907–909.
- (47) Tolan, M. *X-Ray Scattering from Soft-Matter Thin Films*; Springer: Berlin, 1999.
- (48) Kowarik, S.; Gerlach, A.; Sellner, S.; Schreiber, F.; Cavalcanti, L.; Kononov, O. Real-Time Observation of Structural and Orientational Transitions During Growth of Organic Thin Films. *Phys. Rev. Lett.* **2006**, *96*, 125504.
- (49) Barrena, E.; De Oteyza, D. G.; Sellner, S.; Dosch, H.; Ossó, J. O.; Struth, B. In Situ Study of the Growth of Nanodots in Organic Heteroepitaxy. *Phys. Rev. Lett.* **2006**, *97*, 076102.
- (50) De Oteyza, D. G.; Barrena, E.; Ossó, J. O.; Sellner, S.; Dosch, H. Thickness-Dependent Structural Transitions in Fluorinated Copperphthalocyanine (F<sub>16</sub>CuPc) Films. *J. Am. Chem. Soc.* **2006**, *128*, 15052–15053.
- (51) Mannsfeld, S. C. B.; Virkar, A.; Reese, C.; Toney, M. F.; Bao, Z. Precise Structure of Pentacene Monolayers on Amorphous Silicon Oxide and Relation to Charge Transport. *Adv. Mater.* **2009**, *21*, 2294–2298.
- (52) Hayakawa, R.; Zhang, X.; Dosch, H.; Hiroshiba, N.; Chikyow, T.; Wakayama, Y. Stress Release Drives Growth Transition of Quaterylene Thin Films on SiO<sub>2</sub> Surfaces. *J. Phys. Chem. C* **2009**, *113*, 2197–2199.
- (53) Lorch, C.; Banerjee, R.; Frank, C.; Dieterle, J.; Hinderhofer, A.; Gerlach, A.; Schreiber, F. Growth of Competing Crystal Phases of  $\alpha$ -Sexithiophene Studied by Real-Time In Situ X-Ray Scattering. *J. Phys. Chem. C* **2015**, *119*, 819–825.
- (54) Hayakawa, R.; Turak, A.; Zhang, X.; Hiroshiba, N.; Dosch, H.; Chikyow, T.; Wakayama, Y. Strain-Effect for Controlled Growth Mode and Well-Ordered Structure of Quaterylene Thin Films. *J. Chem. Phys.* **2010**, *133*, 034706.
- (55) Hosokai, T.; Mitsuo, N.; Noro, S.; Nakamura, T.; Kera, S.; Sakamoto, K.; Ueno, N. Thickness-Dependent Electronic Properties and Molecular Orientation of Diradical Metal Complex Thin Films Grown on SiO<sub>2</sub>. *Chem. Phys. Lett.* **2010**, *487*, 67–70.
- (56) Gottardi, S.; Toccoli, T.; Iannotta, S.; Bettotti, P.; Cassinese, A.; Barra, M.; Ricciotti, L.; Kubozono, Y. Optimizing Picene Molecular Assembling by Supersonic Molecular Beam Deposition. *J. Phys. Chem. C* **2012**, *116*, 24503–24511.
- (57) Sueyoshi, T.; Fukagawa, H.; Ono, M.; Kera, S.; Ueno, N. Low-Density Band-Gap States in Pentacene Thin Films Probed with Ultrahigh Sensitivity Ultraviolet Photoelectron Spectroscopy. *Appl. Phys. Lett.* **2009**, *95*, 183303.
- (58) Sueyoshi, T.; Kakuta, H.; Ono, M.; Sakamoto, K.; Kera, S.; Ueno, N. Band Gap States of Copper Phthalocyanine Thin Films Induced by Nitrogen Exposure. *Appl. Phys. Lett.* **2010**, *96*, 093303.
- (59) Bussolotti, F.; Kera, S.; Kudo, K.; Kahn, A.; Ueno, N. Gap States in Pentacene Thin Film Induced by Inert Gas Exposure. *Phys. Rev. Lett.* **2013**, *110*, 267602.
- (60) Zu Heringdorf, F.-J. M.; Reuter, M. C.; Tromp, R. M. Growth Dynamics of Pentacene Thin Films. *Nature* **2001**, *412*, 517–520.
- (61) Kowarik, S.; Gerlach, A.; Leitenberger, W.; Hu, J.; Witte, G.; Wöll, C.; Pietsch, U.; Schreiber, F. Energy-Dispersive Reflectivity and GID for Real-Time Growth Studies of Pentacene Thin Films. *Thin Solid Films* **2007**, *515*, 5606–5610.
- (62) Schiefer, S.; Huth, M.; Dobrinevski, A.; Nickel, B. Determination of the Crystal Structure of Substrate-Induced Pentacene Polymorphs in Fiber Structured Thin Films. *J. Am. Chem. Soc.* **2007**, *129*, 10316–10317.
- (63) Ueno, N.; Kera, S.; Sakamoto, K.; Okudaira, K. K. Energy Band and Electron-Vibration Coupling in Organic Thin Films: Photoelectron Spectroscopy as a Powerful Tool for Studying the Charge Transport. *Appl. Phys. A: Mater. Sci. Process.* **2008**, *92*, 495–504.
- (64) Kakuta, H.; Hirahara, T.; Matsuda, I.; Nagao, T.; Hasegawa, S.; Ueno, N.; Sakamoto, K. Electronic Structures of the Highest Occupied Molecular Orbital Bands of a Pentacene Ultrathin Film. *Phys. Rev. Lett.* **2007**, *98*, 247601.
- (65) Ohtomo, M.; Suzuki, T.; Shimada, T.; Hasegawa, T. Band Dispersion of Quasi-single Crystal Thin Film Phase Pentacene Monolayer studied by Angle-Resolved Photoelectron Spectroscopy. *Appl. Phys. Lett.* **2009**, *95*, 123308.
- (66) Yang, J.; Sun, Q.; Yonezawa, K.; Hinderhofer, A.; Gerlach, A.; Broch, K.; Bussolotti, F.; Gao, X.; Li, Y.; Tang, J.; et al. Interface Optimization using Diindenoperylene for C<sub>60</sub> Thin Film Transistors with High Electron Mobility and Stability. *Org. Electron.* **2014**, *15*, 2749–2755.
- (67) Liu, Y.; Ikeda, D.; Nagamatsu, S.; Nishi, T.; Ueno, N.; Kera, S. Impact of Molecular Orbital Distribution on Photoelectron Intensity for Picene Film. *J. Electron Spectrosc. Relat. Phenom.* **2014**, *195*, 287–292.
- (68) Heimel, G.; Salzmann, I.; Duhm, S.; Koch, N. Design of Organic Semiconductors from Molecular Electrostatics. *Chem. Mater.* **2011**, *23*, 359–377.
- (69) Salzmann, I.; Duhm, S.; Heimel, G.; Oehzelt, M.; Kniprath, R.; Johnson, R. L.; Rabe, J. P.; Koch, N. Tuning the Ionization Energy of

Organic Semiconductor Films: The Role of Intramolecular Polar Bonds. *J. Am. Chem. Soc.* **2008**, *130*, 12870–12871.

(70) Chen, W.; Huang, H.; Chen, S.; Huang, Y. L.; Gao, X. Y.; Wee, A. T. S. Molecular Orientation-Dependent Ionization Potential of Organic Thin Films. *Chem. Mater.* **2008**, *20*, 7017–7021.

(71) Yoshida, H.; Sato, N. Grazing-incidence X-ray Diffraction Study of pentacene Thin Films with the Bulk Phase Structure. *Appl. Phys. Lett.* **2006**, *89*, 101919.

(72) Yoshida, H.; Yamada, K.; Tsutsumi, J.; Sato, N. Complete Description of Ionization Energy and Electron Affinity in Organic Solids: Determining Contributions from Electronic Polarization, Energy Band Dispersion, and Molecular Orientation. *Phys. Rev. B: Condens. Matter Mater. Phys.* **2015**, *92*, 075145.

(73) Götzten, J.; Käfer, D.; Wöll, C.; Witte, G. Growth and Structure of Pentacene Films on Graphite: Weak Adhesion as a Key for Epitaxial Film Growth. *Phys. Rev. B: Condens. Matter Mater. Phys.* **2010**, *81*, 085440.

(74) Langner, A.; Hauschild, A.; Fahrenholz, S.; Sokolowski, M. Structural Properties of Tetracene Films on Ag(1 1 1) Investigated by SPA-LEED and TPD. *Surf. Sci.* **2005**, *574*, 153–165.

(75) Yoshida, Y.; Yang, H.; Huang, H.; Guan, S.; Yanagisawa, S.; Yokosuka, T.; Lin, M.; Su, W.; Chang, C.; Hoffmann, G.; et al. Scanning Tunneling Microscopy/Spectroscopy of Picene Thin Films Formed on Ag(111). *J. Chem. Phys.* **2014**, *141*, 114701.

(76) Beyer, P.; Breuer, T.; Ndiaye, S.; Zykov, A.; Viertel, A.; Gensler, M.; Rabe, J. P.; Hecht, S.; Witte, G.; Kowarik, S. Lattice Matching as the Determining Factor for Molecular Tilt and Multilayer Growth Mode of the Nanographene Hexa-peri-hexabenzocoronene. *ACS Appl. Mater. Interfaces* **2014**, *6*, 21484–21493.

(77) Inokuchi, H. The Discovery of Organic Semiconductors. Its Light and Shadow. *Org. Electron.* **2006**, *7*, 62–76.

(78) Nakamura, M.; Morita, Y.; Mori, Y.; Ishitani, A.; Tokumoto, H. Molecular Arrangement of Copper Phthalocyanine on Hydrogen-Terminated Si(111): Influence of Surface Roughness. *J. Vac. Sci. Technol., B: Microelectron. Process. Phenom.* **1996**, *14*, 1109–113.

(79) Käfer, D.; Ruppel, L.; Witte, G. Growth of Pentacene on Clean and Modified Gold Surfaces. *Phys. Rev. B: Condens. Matter Mater. Phys.* **2007**, *75*, 085309.

(80) Peisert, H.; Biswas, I.; Knupfer, M.; Chassé, T. Orientation and Electronic Properties of Phthalocyanines on Polycrystalline Substrates. *Phys. Status Solidi B* **2009**, *246*, 1529–1545.